AEGIS/AD-6 status/progress report for 2009

The AEGIS/AD-6 collaboration:
I. Boscolo[1], F. Castelli[1], S. Cialdi[1], G. Consolati[1], R. Ferragut[1],
M. Giammarchi[1], D.Trezzi[1], F. Villa[1], M. Sacerdoti[1], U. Warring[5],
G. Testera[2], C. Carraro[2], C. Canali[2], S. Zavatarell[2], R. Vaccarone[2],
L. DiNoto[2], V. Lagomarsino[2], D. Krasnicky[2], G. Manuzio[2],
M. Prevedelli[3], G. Ferrari[3], S. Mariazzi[4], R. Brusa[4], D. Fabris[4],
M. Lunardon[4], S. Mariazzi[4], S. Moretto[4], G. Nebbia[4], S. Pesente[4],
G. Viesti[4], A. Kellerbauer[5], A.S. Belov[6], S.N. Gninenko[6], V.A. Matveev[6],
G. Bonomi[7], L. Dassa[7], A. Fontana[7], C. Riccardi[7], A. Rotondi[7],
A. Zenoni[7], D. Sillou[8], P. Nedelec[9], N. Djourelov[10], L. Cabaret[11],
D. Comparat[11], M. Oberthaler[12], F. Haupert[12], P. Bräunig[12],
M. Doser[13], D. Perini[13], A. Dudarev[13], J. Bremer[13], G. Burghart[13],
T. Eisel[13], F. Haug[13], I. Al-Qaradawi[14], L. Jorgensen[14],
S. Hogan[15], F. Merkt[15], H. Sadake[16], O. Rohne[16], J. P. Hansen[16],
V. Petraček[17], H. Stroke[17], G. Gribakin,[18] H. Walters[18]
[1]University and Polytecnico of Milano, [2]INFN of Genoa, [3]INFN Firenze
[4]INFN Trento/Padova, [5]MPI-K, [6]INR, [7]INFN Pavia/Brescia, [8]LAPP,
[9]University of Lyon, [10]INRNE, [11]Laboratoire Aimé Cotton,
[12]University of Heidelberg, [13]CERN [14]Qatar University, [15]ETH Zürich,
[16]University of Oslo, [17]Czech Technical University, [18]New York University,
[19]Queen's University Belfast

1. Introduction and Overview

The primary scientific goal of AEGIS is the direct measurement of the Earth's local gravitational acceleration g on $\bar{H}$. In a first phase of the experiment, a gravity measurement with 1% relative precision will be carried out by observing the vertical displacement (using a high-resolution position sensitive detector) of the shadow image produced by an $\bar{H}$ beam, formed by its passage though a Moiré deflectometer, the classical counterpart of a matter wave interferometer. This measurement will represent the first direct determination of the effect of gravity on antimatter.

The essential steps leading to the production of a pulsed cold beam of $\bar{H}$ and the measurement of g with AEGIS are the following (Fig. 1):

- Production of positrons (e^+) from a Surko-type source and accumulator;
- Capture and accumulation of $\bar{p}$ from the AD in a cylindrical Penning trap;
- Cooling of the $\bar{p}$ to sub-K temperatures
- Production of positronium (Ps) by bombardment of a cryogenic nanoporous material with an intense e^+ pulse;
- Excitation of the Ps to a Rydberg state with principal quantum number n = 30 ∼ 40;
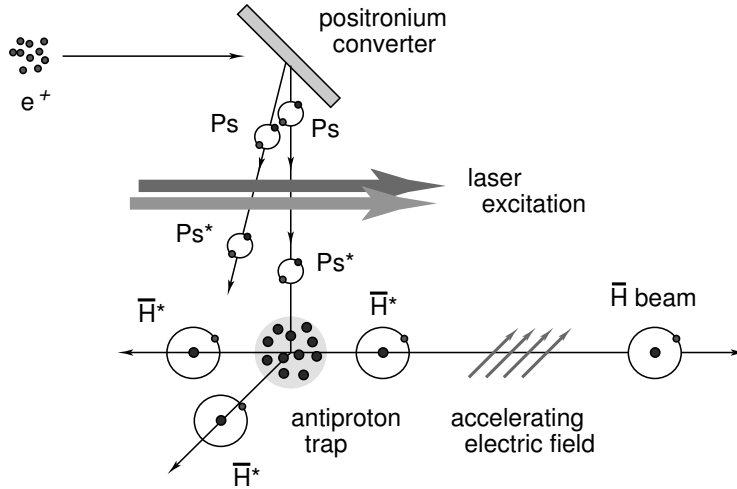- Pulsed formation of $\bar{H}$ by resonant charge exchange between Rydberg Ps and cold $\bar{p}$;

Figure 1. Proposed method for the production of a pulsed beam of cold $\bar{H}$ atoms.

- Pulsed formation of an $\bar{H}$ beam by Stark acceleration with inhomogeneous electric fields;
- Determination of g in a two-grating Moiré deflectometer coupled with a position-sensitive detector.

The proposal submitted to the SPSC, and which was approved in December 2008 [1], is based on achieving these steps. The feasibility of the first two points had been conclusively demonstrated by the ATHENA and ATRAP collaborations (see, in particular [2, 3]), but the remaining points, while based on reasonable extrapolations of known results or calculations, remained to be validated, and only an initial technical design was available at that time.

In the following, we will discuss the remaining aspects of the proposed technique in more detail, point out the advances achieved in 2009, and give an overview of the questions that remain open.

1.1. Antihydrogen recombination and beam formation

An $\bar{H}$ recombination scheme based on resonant charge exchange with Ps was first proposed almost twenty years ago [4]. The reaction proceeds according to the equation

$$Ps^* + \bar{p} \rightarrow \bar{H}^* + e^- \tag{1}$$

where the star denotes a highly excited Rydberg state. This reaction owes its appeal to the fact that the cross-section scales approximately with the fourth power of the principal quantum number. In addition, it creates $\bar{H}$ in a narrow and well-defined band of final states. Most importantly, $\bar{H}$ formed with $\bar{p}$ at rest is created with a velocity distribution dominated by the $\bar{p}$ temperature, hence the surrounding (cryogenic) environment [5]. This is in stark contrast to the rather high $\bar{H}$ temperature observed when using the nested-well technique pioneered by ATRAP and ATHENA [6, 7]. Our proposed technique is conceptually similar to a charge exchange technique based on Rydberg cesium [8] which has been successfully demonstrated by ATRAP [9], but offers greater control of the final state distribution of $\bar{H}$ and, more importantly, allows pulsed production of $\bar{H}$.

The principle is illustrated in Fig. 1. The Ps emitted from the porous insulator material are excited to Rydberg states. They then traverse a Penning trap region in which $\sim 10^5 \bar{p}$ have

been accumulated, stored and cooled to O(100 mK). The low temperature requirement on the antiprotons comes from the requirement that the antihydrogen atoms that will be formed will have a velocity that is low compared to the velocity of several 100 m/s that they will achieve after acceleration. To reach such a low temperature, the Penning trap is coupled to a 50 mK dilution refrigerator, and the antiprotons are coupled to the low temperature environment by embedding them in an electron plasma. The later will cool through synchrotron radiation, as well as through a tuned circuit; furthermore, evaporative cooling of the pre-cooled antiprotons is being envisaged. The charge exchange cross-section is very large ($\sim 10^7 \mathring{A}^2$ for n = 35) and reaches a maximum when the e^+ and $\bar{p}$ relative velocities are matched. Taking into account the corresponding kinetic energy, as well as a smaller contribution due to converted internal energy, $\bar{H}$ is created at velocities of $25 \sim 80~ms^{-1}$.

While neutral atoms are not sensitive (to first order) to constant electric fields, they do experience a force when their electric dipole moment is exposed to an electric-field gradient. Since the dipole moment scales approximately with the square of the principal quantum number, Rydberg atoms are especially amenable to being manipulated in this way. Such so-called Stark acceleration (and deceleration) has been successfully demonstrated, among others, by one of the AEGIS groups with (ordinary) hydrogen after excitation to the n = 22, 23, 24 states [10, 11]. In these experiments, accelerations of $2 \times 10^8 ms^{-2}$ were achieved using two pairs of electrodes at right angles to each other. A hydrogen beam traveling at 700 ms^{-1} was stopped within 5 μs over a distance of only 1.8 mm. We intend to use a similar field configuration, generated by axially split electrodes within the cylindrical geometry of a Penning trap, to accelerate the formed $\bar{H}$ atoms to about 400 ms^{-1} in the direction of the deflectometer apparatus.

1.2. Gravity measurement

In matter wave interferometers of the Mach-Zehnder type [12, 13], three identical gratings are placed at equal distances L from each other. The first two gratings produce an interference pattern at the location of the third. That pattern has the same period d as the gratings, and its position perpendicular to the diffracted particle beam can be determined precisely by displacing the third grating and recording the overall transmission with a particle detector. Under the influence of gravity, the interference pattern is vertically displaced (it falls) by a distance

$$\delta x = -gT^2 \tag{2}$$

where g is the local gravitational acceleration and T is the time of flight L/v between each pair of gratings of a particle beam traveling at velocity v.

Contrary to such true interferometers, which place a very stringent limit on the acceptable beam divergence (and thus antihydrogen temperature at production), the so-called Moiré deflectometer, in which diffraction on the gratings is replaced by a (classical) shadow pattern of those particles that converge onto the third grating, works in the classical regime. Interestingly, the gross characteristics of the interferometer are retained [14], in particular, the vertical displacement of the interference pattern according to Eq. (2). A three-grating Moiré deflectometer has been used to measure the local gravitational acceleration to a relative precision of 2×10^{-4} with a beam of argon atoms traveling at an average velocity of 750 ms^{-1} [14]. In departing from the three-grating deflectometer, we intend to replace the third grating by a position-sensitive silicon strip detector (see Fig. 2). Antihydrogen atoms impacting on the detector plane annihilate, and the impact point can be reconstructed by means of the energy deposited locally by the annihilation products.

The value of g is extracted from two primary observables (time of flight T and vertical displacement of the fringe pattern δx). The periodic nature of the arrangement means that for a given value of T, the impact point will have dropped by a well-defined amount $\delta x(T)$, modulo the grating period. By varying the accelerating field gradient (and thus varying the
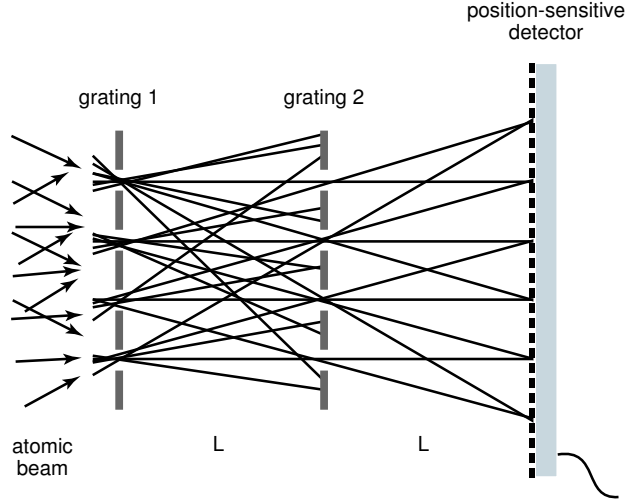
Figure 2. Schematic of the principle of the Moiré deflectometer consisting of two gratings coupled to a position-sensitive detector.

velocity of the antihydrogen atoms), or simply through the spread in velocity of the ensemble of antihydrogen atoms, the quadratic dependence of δx on T is probed.

Our simulations have shown that in order to perform a measurement of g to 1% relative precision, about 10^5 H atoms at a temperature of 100 mK will be required. equivalent to several months of data taking at the AD. In these simulations, a grating period of 80 μm was used, and a finite detector resolution of 10 μm was taken into account.

2. Preparatory work and methodological developments

2.1. Technical design

The AD-6 experiment will be sited in the last available area of the AD hall, the DEM zone. The dimensions of the zone, but also beam and safety requirements, impose a number of constraints on the overall layout of the experiment, as well as on specific components of the apparatus.

The overall layout has moved from a horizontally planar configuration (which would have had the positron accumulator and the main magnet side-by-side) to a configuration in which the positron accumulator is positioned above the antiproton beam line (Figs.3 and 4).

The main apparatus consists of two magnets: a 5T magnet (where field strength is important in maximizing the trapping efficiency for antiprotons delivered from the AD), and a 1T magnet in which the antihydrogen beam will be produced. The custom design integrates the super-conducting magnets and their cryostats with the dilution refrigerator and its cryostats, as well as allowing access from the two sides (antiproton and positron injection on the upstream side and antihydrogen beam extraction on the downstream side) as well as in the region between the two magnets (cabling and diagnostics). Laser light for Positronium excitation is injected from the downstream side of the 1T magnet.

Achieving the sub-Kelvin antiproton temperatures required to form a slow-moving beam of antihydrogen atoms requires, in addition to the presence of a dilution refrigerator, a very high homogeneity of the 1T field in which the antiprotons will be stored and cooled. The design of the magnet system achieves these two objectives, and provides a smoothly decreasing transition between the 5T and the 1T fields, which allows a loss-free transfer of antiprotons and positrons from the 5T trapping region to the 1T central region. Fig. 6 shows the field values along the axis
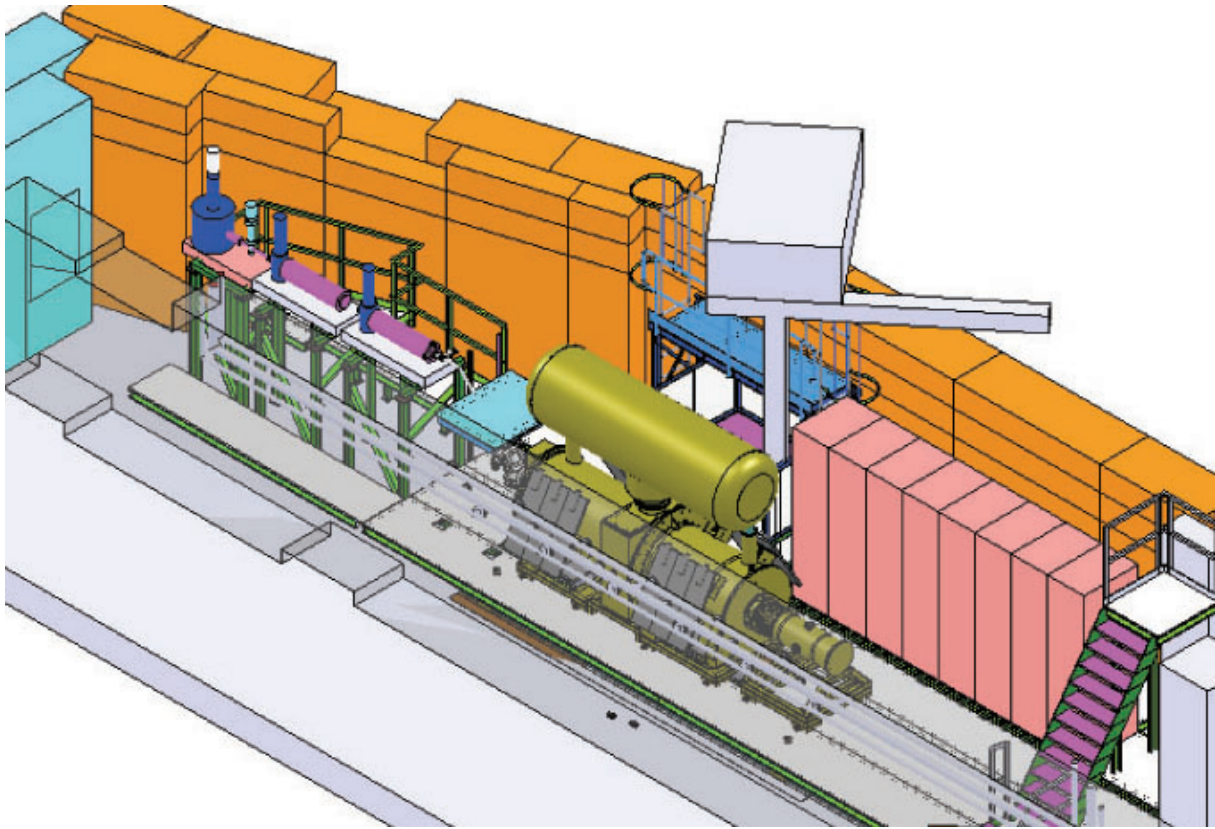
Figure 3. Overall layout of the different components of the experiment in the DEM zone.

of the apparatus, as well as the homogeneity that can be achieved. This also requires great care in the construction, and it has thus been decided to build these two magnets at CERN. A custom-built device to wind the magnets has been constructed, and is undergoing final tests before construction of the magnets commences at the beginning of February. Similarly, construction of the cryostat vessels that will house the magnets is well under way, and it is planned to test the completed coils, and measure the field homogeneity, towards the middle of the year in the CERN cryogenics lab.

2.2. Positron accumulator and transfer

Once the overall design was completed, an order was placed with First Point Scientific for a custom-modified positron accumulator, whose delivery is scheduled for the second half of 2010. These modifications are minor (taking into account the lack of free space underneath the accumulator, which houses the antiproton injection line), and could be easily accommodated by the company.

Similarly, a provisional order for the ^{22}Na source with IThemba was placed in the second half of 2009, ensuring delivery of the source in fall of 2010; the order will be finalized in spring, as required to account for IThemba's accountancy cycle.

Positrons are transfered from the 0.1T accumulator into the 5T magnet through a transfer section, requiring care to ensure lossless passage. The design of this transfer line (hardware, trajectory simulations and diagnostics) is completed, orders for the required hardware are being placed, and construction of the mechanics are scheduled to start in spring.
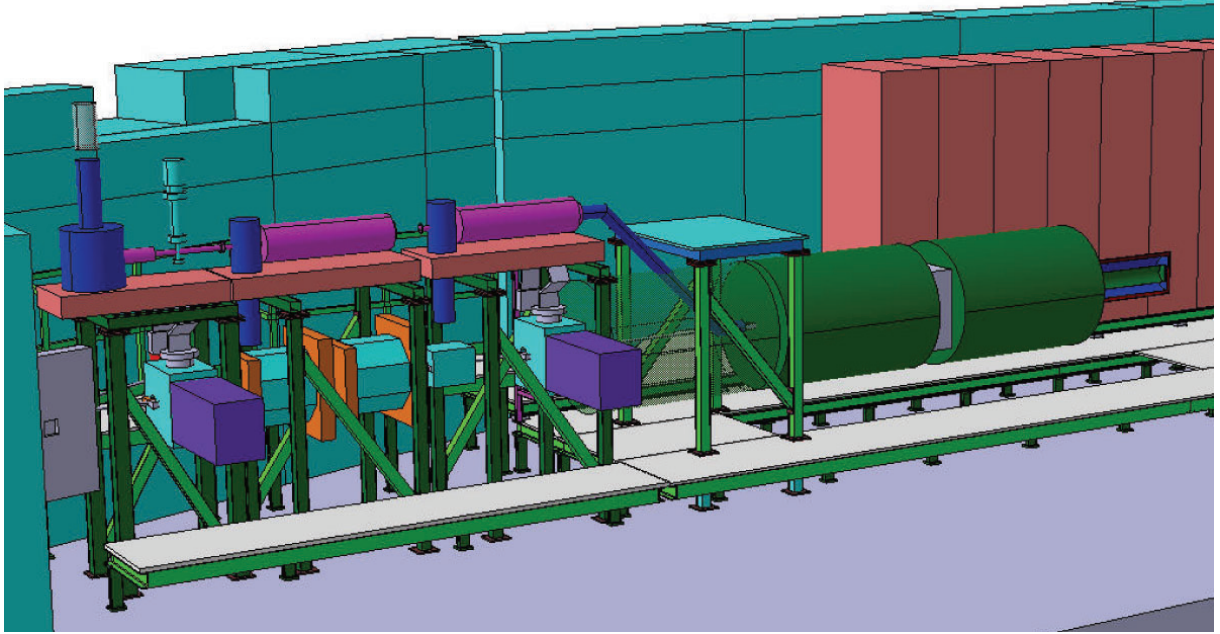
Figure 4. Side view of the antiproton beam line and of the accumulator above it, followed by the 5T and the 1T magnets.

2.3. Plasma manipulations

The design of the experiment foresees injecting antiprotons (from the AD) and positrons (from the positron accumulator) into the 5T magnet, and then transferring both into the 1T magnet into an intermediate storage region. From there, the antiprotons are transfered into the ultra-cold region, while the positrons require shifting off-axis into the stack of electrodes that run parallel to those housing the ultra-cold antiprotons, in order to subsequently extract them onto the positronium target.

While such a radial shift has been demonstrated [15], we needed to reproduce and gain experience with the procedure, and develop diagnostic tools that would allow us to monitor the process. A test set-up in Genoa using electrons in a 2 T magnet was used to attempt the procedure.

In Fig. 7 the experimental apparatus is described: a cylindrical Penning trap is placed inside a vaccum chamber at ambient temperature ($P < 10^{-10}mbar$). A superconducting magnet superimposes a magnetic field ($B = 2T$) along the trap axis. Each electrode can be polarized independently. One electrode of the trap is sectorized into 4 parts. An optical diagnostic is mounted on one end of the trap and a faraday cup on the opposite side. All the tests reported here have been performed using a plasma of electrons. Electrons are provided by a barium-oxide cathode, typically 10^8 electrons are confined in the trap. After applying a "rotating wall" procedure, the plasma reaches a final density of $\simeq 10^8 e^-/cm^3$.

At this point the diocotron excitation signal can be applied to one sector of the split electrode. The driving signal increases its amplitude and frequency within the first $10ms$, then it is kept at a constant frequency ($\simeq 10kHz$) and amplitude ($\simeq 2V$). During this time the plasma enters into autoresonance with the driving signal itself and starts to move along a cicular path around
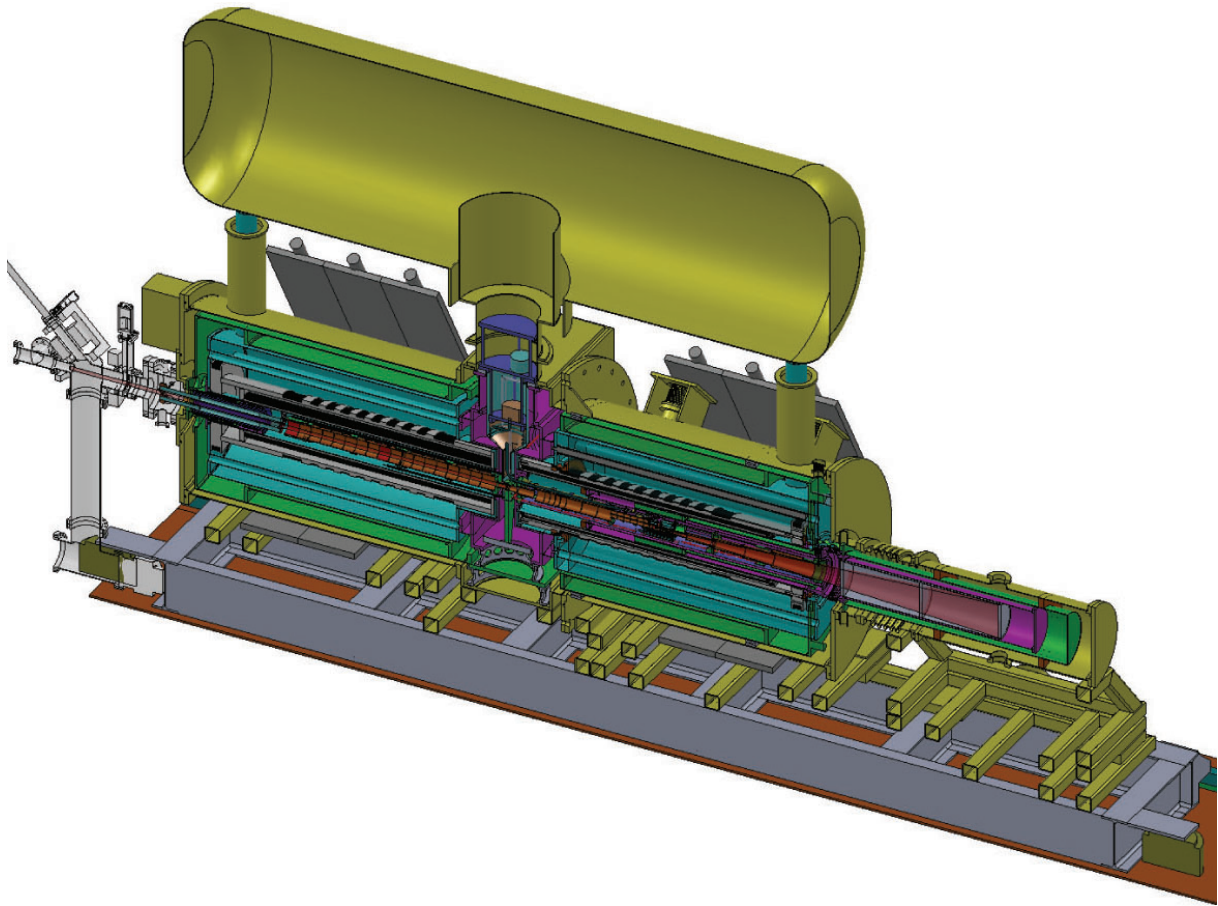
Figure 5. Cross-section through the 5T and 1T magnets, showing the details of the cryostats, dilution refrigerator and electrodes.

the trap axis. The phase of the motion of the plasma is the same as of the driving signal. An appropriately timed fast pulse synchronized with the driving signal defines the angle at which the plasma is ejected from the trap. This procedure is schematically described in Fig. 8.

Figure 9 shows the results obtained following the experimental procedure described above. On the left plot is shown the radius to which the plasma is displaced as a function of the driving signal; the plot on the right shows the angular positions of the plasma with respect to the phase of the driving signal at the moment of the dump.

It is interesting to note that in this series of measurements a complete control over the final positioning of the plasma is obtained, since the frequency unambiguously determines the final radial position of the plasma while it is possible to control the angular position of the plasma with a proper timing of the dump pulse. During the diocotron excitation the radius of the plasma increases by less than 10%, while no particles are lost. In conclusion the measurements described here meet the requirements necessary in the AEGIS experiments.

In the next step a cylindrical trap almost identical to the one that will be used in AEGIS will be installed in the Genova apparatus. In this new trap the off-axis re-trapping after the diocotron exitation will be investigated.
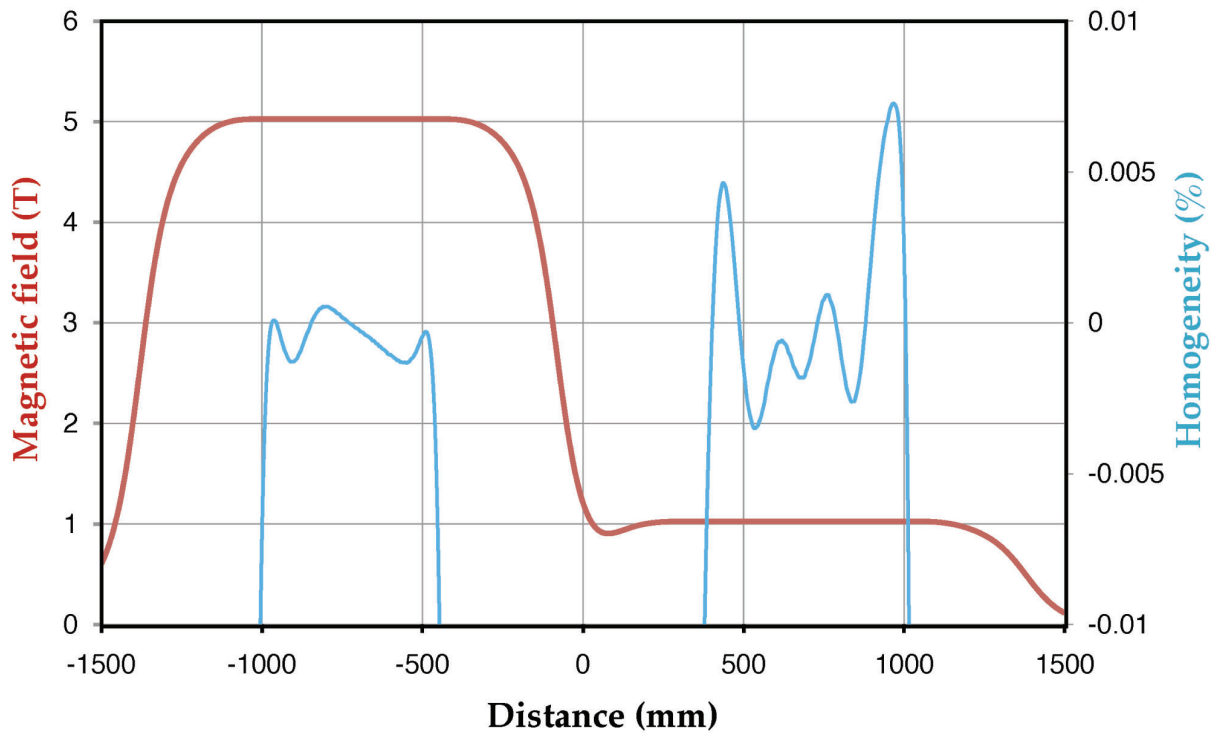
Figure 6. Field value along the axis (in red); field homogeneity in the 5T and 1T region (in blue); antiprotons are trapped in the 5T magnetic field, and are cooled in the 1T region. The distance is with respect to the center of the transfer region between the two magnets.
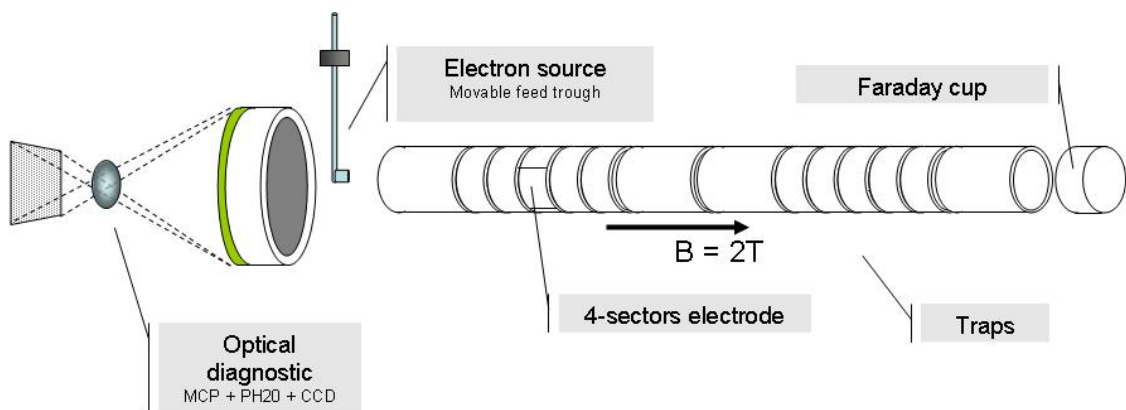

Figure 7. The apparatus used to perform tests on plasma manipulation in the laboratory of INFN of Genova. A cylindrical Penning trap is placed inside a superconducting magnet. On the left side an optical diagnostic tool (composed of an MCP, a phosphor screen and a CCD camera) is used to obtain information about the plasma position and radious. On the right side a faraday cup is used to detect the number of electrons.
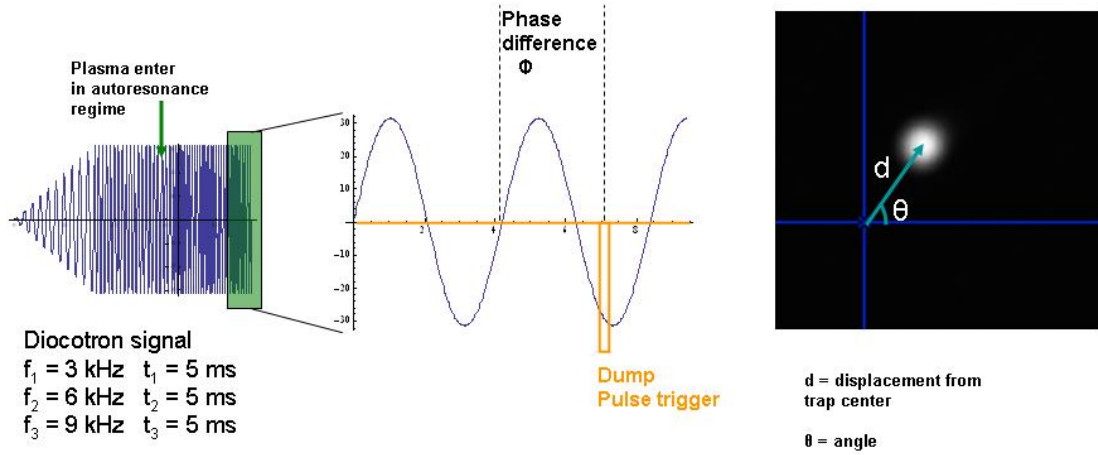
Figure 8. The scheme of the diocotron excitation procedure is drawn on the left. After bringing the plasma into autoresonance with the driving signal, a fast dump precisely synchronized with the drive ejects the plasma onto the MCP. On the right side, a plasma radially shifted out from the center of the trap is detected with the optical diagnostic.
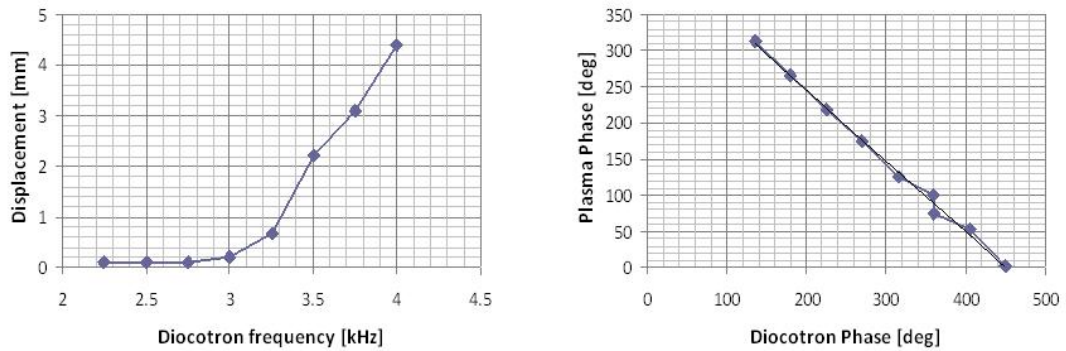

Figure 9. Left plot: radial displacement of the plasma from the center of the trap as a function of the diocotron driving frequency. Right plot: final angular position of the plasma as a function of the drive phase at the moment of the dump.

2.4. Positronium production

In recent years, the potential for nanoporous insulator materials to be used as highly efficient Ps converters has been recognized, and the relevant formation mechanisms have been studied extensively [16]. When e^+ are implanted into such a material at kinetic energies ranging from several 100 eV to a few keV, they scatter off atoms and electrons in the bulk and are slowed to eV energies within a few ps. With efficiencies ranging from 10% to 50%, the slow e^+ capture either bound e^- or those liberated in prior collisions and form Ps. In the pores, Ps repeatedly bounces off the cavity walls and eventually approaches complete thermalization with the target material. The overall ortho-Ps yield as well as the final velocity distribution depend upon the characteristics of the target material (in particular, its pore structure), the implantation depth, and the target temperature.

For the AEGIS experiment, the overall yield and the precise degree of thermalization is

critical, since at too low a Ps temperature, annihilation in the target material will dominate, while at too high a Ps temperature, the subsequent charge exchange cross section (to form $\bar{H}$) drops rapidly [17]. By carefully tailoring the topology of the target material's pores however, a degree of control appears possible [18].

In 2009, a number of advances have been achieved on the production and characterization of Ps:

- a novel target to convert implanted positrons in positronium was found and produced.
- a Time of Flight (TOF) apparatus for measuring the Ps velocity was designed and set up at the Trento continuous slow positron beam.
- TOF measurements with the target held at cryogenic temperature were done. 3% of implanted positrons in our novel target held at 150 K were found to be emitted into vacuum after thermalizing to the target temperature.
- a new TOF chamber is under design. This new chamber will be mounted at the NEPOMUC intense positron source at the research reactor FRMII of Munich. Measurements with this intense positron source will be faster, allowing to measure TOF spectra at target temperatures down to 10 K or even 4 K.

Novel positronium converter   Positronium is efficiently formed in porous silica based materials and if the porosities are connected towards the surface a fraction of the formed Ps can escape into the vacuum. Up to now several groups have studied porous silica materials with disordered and connected porosities. Ps is emitted into pores with energy of few eV, and cools down by collisions with the wall of the pores. Positronium was found to thermalize at room temperature. No measurements have been reported at cryogenic temperature.

We have followed a different route looking for a novel structure with ordered nano-channels perpendicular to the surface. Nano-channels have been produced by selective etching in silicon and oxidized in air at different temperatures and times. A scanning electron microscopy picture of the converter surface is shown in Fig. 10. In that sample, holes of 5-8 nm in diameter are present, and are spaced by about the same distance of 5-8 nm.

The synthesis of the converter was optimized by maximizing the positronium yield. A sketch of the converter is shown in Fig. 10. The high positronium yield of this system is due to the following processes. Implanted positrons thermalize in silicon. Due to the high diffusion length (200 nm in Si), a big fraction of thermalized positrons reaches the Si/SiO_2 interface. Positrons are energetically favored to pass from Si to the silicon oxide covering the walls of the channels. In the silicon oxide, positrons form Ps that is emitted after a very small path (few nm of silica) in the channels. This target has many advantages with respect to silica with disordered channels: a) the diameter of the channels can be tuned. This is important if Ps at very low velocity is to be obtained. With small channel diameters (lower than 5 nm) Ps quantum confining does not allow Ps thermalization at cryogenic temperature. b) The channels allow a very high fraction of Ps to escape into vacuum from the sample. c) The silicon converter is expected to be less sensitive to charging effects and damage effects under positron bombardment. d) Positronium velocity in vacuum may be tuned by a suitable choice of the positron implantation energy and the sample temperature.

A variety of further materials have also been studied in Milano, including Vycor glasses, MOFs, Germanate porous glasses and Aerogel/Xerogel materials [20] and elsewhere, particularly porous anodic alumina Al2O3 [21]. In particular, Xerogel materials have shown to be very promising in terms of producing a high Ps yield. The results of these tests have suggested that low density (85 mg/cm^3) Xerogel, developed by NASA for space gas trapping applications, may be the most promising sample to focus further research on. Tests of capping of the Xerogel samples (to determine the fraction of Ps emitted into the vacuum) have subsequently been
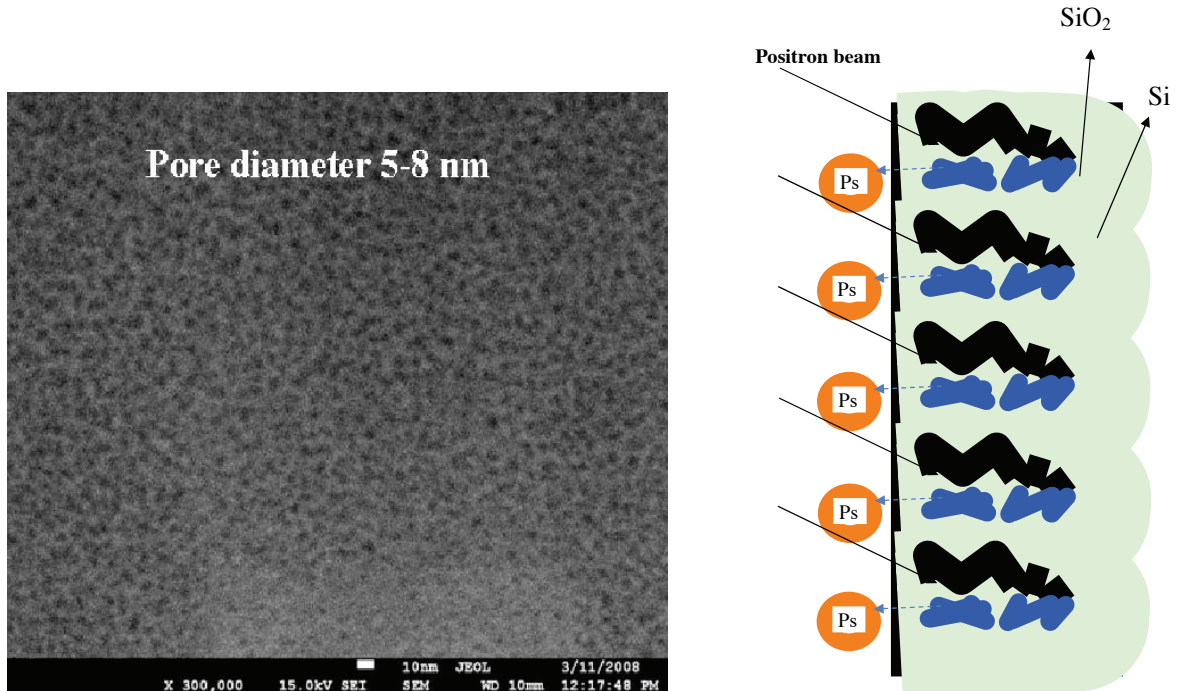
Figure 10. Left plot: SEM picture of the converter surface with 5-8 nm pores. Right plot: Sketch of the Si converter in which nano-channels are produced. The surfaces of the nano-channels are oxidized in air with the converter held at some hundreds degrees for some hours.

made. An Al capping was deposited on the surface with the goal of assessing the behaviour of the sample tested under such conditions. The result is a clear drop in the low-energy part of the spectrum, indicating that Ps is emitted into vacuum from the (uncapped) Xerogel sample. This material guarantees one of the highest Ps yields ever observed and at the same time exhibits a significant emission from the surface. This is also confirmed by lifetime studies that have been performed by our group in Munich [20]. We are now in the process of refining emission measurements and preparing to perform velocity measurements of the emitted Positronium.

Positronium Yield and Ps velocity: In the following the data obtained with the converter held at 150 K will be presented and discussed. In Fig.11a), the Positronium yield (F3γ) as obtained by 3γ-Ps annihilation measurements is shown. A fitting procedure, based on a Ps diffusion model, points out that the F3γ positronium fraction shown in fig. 11a) at each positron implantation energy corresponds almost completely to Ps out-diffusing into vacuum from the sample (only 0.5% annihilate into the channels). A maximum yield of about 40% is obtained at energies of few keV. At higher positron implantation energies the differences between the F3γ at energy E and the maximum yield, gives the percentage of Ps annihilating by pick-off into two gamma rays before reaching the vacuum.

It must be pointed out that at a positron implantation energy of 7 keV more than 20% of the implanted positrons give rise to Ps out-diffusing into the vacuum. Time of Flight measurements of Ps are mandatory to know if Ps out diffusing in vacuum is thermalized at the converter

temperature.

In the set up at Trento the starting signal was given by secondary electrons emitted by impinging positrons on the converter. The electrons were detected by a channeltron electron multiplier. The stop signal was given by the Ps in flight annihilation gamma rays detected by a NaITl detector placed behind a 5 mm wide, 100 mm long slit obtained with a tungsten shield. The centre of the slit was placed 8.9 mm away from the converter surface. For each TOF spectrum with the Trento positron beam (2×10^4 e$^+$/s), 14 days of measurements were necessary: about 2000 Ps annihilations were detected in the small solid angle subtended by the NaITl detector. The FWHM of the prompt peak was 23 ns.

In Fig.11a) the TOF spectrum is shown after background subtraction and smoothing on 64 points. The asymmetric shape of the TOF spectrum with a fast Ps component (short times) reflects the Ps out-diffusing from straight channels. Many Ps atoms are emitted from the channels after only few interactions with the walls of the channels and therefore with high velocity. The thermalized fraction of Ps at 150 K can be obtained by the area subtended by the TOF spectrum from the time $t_M = z_0/v_{th}$ (where $v_{th} = \sqrt{3k_BT/m_0}$ is the $o-$Ps velocity corresponding to the sample temperature T, and k_B is the Boltzman constant) to the end of the distribution. It is found that 2.5% of implanted positrons give Ps into vacuum with thermal velocity corresponding to 150 K. This is the right velocity for an efficient charge exchange process between Ps and antiprotons to form antihydrogen. With the present converter, with a typical bunch of 2×10^8 e$^+$, about 5×10^6 cooled Ps atoms in vacuum can be obtained. In Fig.11b) the Ps energy spectrum of the Ps emitted into vacuum is reported. The energy spectrum is obtained by the data of Fig.11c). The spectrum is well fitted by two exponentials and shows that there are two distinct beam Maxwellian distributions. The one at T=145 $\pm$ 10 K corresponds to thermalized Ps atoms. It must be stressed that this is the first result reporting thermalization of Ps from regular nano-channels at a temperature lower than room temperature. Two papers based on these results have been submitted. In the present apparatus, due to the long time needed for acquiring Ps TOF spectra, 150 K is the lowest accessible temperature. Below 150 K at 10^{-9} Torr (the vacuum in our chamber) condensation of water on the surface of the converter starts. To go below these temperatures an apparatus, to be moved at the NEPOMUC high intensity source at FRMII, is under construction.

TOF chamber for NEPOMUC intense positron source   At the end of this month a proposal to set up a TOF apparatus for measuring Ps velocity at NEPOMUC will be submitted at the FRMII facility of Munich. The apparatus is under construction at Trento. The apparatus characteristics will be:

 (i) Two channeltrons with wide solid angle acceptance for detecting secondary electrons.

 (ii) from four to six to eleven NaITl detectors of 3 cm in diameter

(iii) the apparatus will also allow measurements of the Ps emission angles from the converter.

With this detector's parameters, and taking into account that the NEPOMUC source has a positron beam of 10^7 e$^+$/s, it will be possible to acquire one TOF spectrum in 15 min. Ps velocity measurements down to 10 K and, not less important, Ps emission angle measurements will be possible with this new apparatus.

2.5. Positronium excitation

Antihydrogen production by charge exchange reaction between Positronium (Ps) atoms and antiprotons is the main process considered for antimatter production in Aegis. Since the cross section for this reaction depends roughly on n^4, we are developing an efficient excitation system to pump Ps atoms up to high-n levels (Rydberg levels). The system is under development and
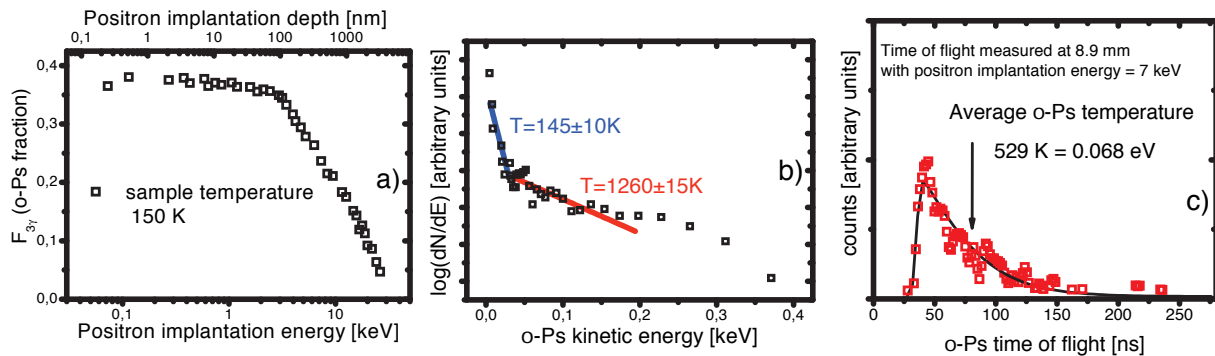
Figure 11. a) Positronium fraction relative to the number of implanted positrons; b) energy spectrum of Ps emitted in vacuum, obtained from the data of plot c; c) TOF spectrum of Ps

will be implemented in the area where a Ps cloud is produced by positrons hitting a porous silica target in a Penning-Malmberg trap with a relatively strong uniform magnetic field (1 T). Our experimental strategy involves exciting Positronium into Rydberg states in two steps, one from $n = 1$ to $n = 3$, which involves radiation at 205 nm, and a second from $n = 3$ to $n = 20 \ldots 30$, involving radiation in the range from 1650 nm to 1700 nm. Two groups have been working on the implementation of the two laser sources with which we will excite positronium towards Rydberg states, the groups in Milan and in Florence. While the Milan group is responsible for the realization of the 1670 nm laser, the group in Florence will realize the 205 nm laser. The two laser sources share similar requirements in terms of spectral properties, as discussed in [19], and adopt related technical solutions.

The main features of this two-step excitation are the significant Doppler effect for the first transition and the modifications due to Zeeman and motional Stark effects on the high-n sublevel structure [19]. The pump laser of the whole system will be a 300 mJ Q-switched Nd:YAG laser delivering a 4 ns pulse. The radiations are produced through second-order polarization in optical crystals (see fig. 12). The 205 nm radiation for the first transition is obtained by summing in a non-linear BBO crystal the 266 nm fourth-harmonic of the 1064 nm Nd:YAG pulse and the 894 nm radiation generated in an OPG by down-conversion of the second-harmonic of the same laser. The other wavelength (around 1670 nm) is generated in a single step by an OPG starting from the same pump laser and then amplified by an OPA system.

The system has been completely designed and is partly completed. Tests are under way in Milan on the part responsible for the second transition. We have exceeded the energy required to saturate this second transition of 174 μJ [19], having currently reached 1,000 μJ after an OPA using a temporary Nd:YAG laser of only 80 mJ energy per pulse. We are currently studying the stability in space and in energy of the produced pulse with the goal of optimizing the system.

The laser system at 205 nm responsible for the excitation $n = 1 \rightarrow n = 3$ has the following requirements:

(i) spectral bandwidth larger than 150 GHz RMS, mainly accounting for the the Doppler broadening, with a continuum, non-discrete, spectrum (see the discussion in [19]),

(ii) a pulse duration shorter than 10 ns,

(iii) an integrated energy in the range of 100 μJ or lager.

The requirements on the spectral properties and the pulse duration are easily fulfilled by using an optical parametric generator (OPG) pumped by a Q-switched pump laser, but those on the wavelength and the energy per pulse are not as trivial to be fulfilled. In fact producing 205 nm photons by direct parametric down-conversion is not realistic because of the lack of suitable pump lasers at wavelengths shorter than 205 nm. Alternative approaches based on harmonic generation, such as frequency doubling or tripling, of parametrically down-converted photons at longer wavelength are not viable mainly because of the limited efficiency attainable in the harmonic process. Given these constraints we will consider a different approach based both on parametric down-conversion and frequency summing processes. Here the first requirement is satisfied by generating radiation at 894 nm with an OPG pumped by a nanosecond frequency doubled Nd:YAG laser at 532 nm. Subsequently the 894 nm light is frequency summed to the second harmonic of the same pump laser, at a wavelength of 266 nm, hence generating 205 nm radiation. Compared to the case of direct harmonic generation of the OPG-generated radiation, with our approach the conversion process towards 205 nm is considerably more effective because of the large amount of energy available at 266 nm with nanosecond lasers which boosts the nonlinear conversion towards the deep UV. From the spectral point of view the frequency summing process consists in adding the continuous spectrum from the OPG, to the comb-like spectrum of the 266 nm radiation (obtained as the fourth harmonic of a Q-switched Nd:YAG lasers), hence resulting in the required continuous spectrum peaked at 205 nm.

A sketch of the laser setup under development is depicted in Fig. 12. Starting from the same pump laser of the 1670 nm laser under construction in Milan, a beam-splitter conveys about half of the energy to a first frequency doubling stage based on a BBO crystal (BBO1 in Fig. 12) to generate about 75 mJ at a wavelength of 532 nm. A visible beam splitter sends about 3 mJ of the 532 nm pulse to the OPG generating 894 nm radiation, while the remainder is sent to a second frequency doubling stage, based again on a BBO nonlinear crystal (BBO2), which converts about 15 mJ to 266 nm. The OPG is based on a 30 mm long periodically-poled KTP crystal which ensures an efficiency on the conversion towards 894 nm of about 10 % when pumping with pulses of 3 mJ, hence resulting in pulses of about 300 μJ in the infrared. Finally, the frequency summing stage is composed by a dichroic mirror superposing the radiations at 894 nm and 266 nm, which is followed by a third BBO crystal (BBO3 in Fig. 12) cut to satisfy the type-I phase matching condition for the process 894 nm + 266 nm → 205 nm, and 3 mm long in order to insure a nonlinear conversion bandwidth larger than 150 GHz for frequency tuning of the infrared radiation. In the end we expect to obtain about 400 μJ at 205 nm on a spectrum fulfilling the specifications as discussed above.

We expect to start the tests on the 205 nm laser in the course of February 2010 as all the required elements (pumping laser, nonlinear crystals, general purpose optics and electronics) are already available in Florence, or are expected to be delivered by the end of January 2010.

2.6. Dilution refrigerator

Achieving a sufficiently cold cloud of antiprotons is a central requirement of the experiment; the target antiproton temperature is 100 mK.

The overall cryogenic system of the AEGIS experiment is very complex, but in general state of the art. However, cooling the antiprotons to ultra cold temperatures is a challenge. The antiprotons will be cooled within a Penning trap, which will be formed by several electrodes. These ultra cold electrodes need to be cooled down to 100 mK and will therefore be mounted directly on the heat sink of a dilution refrigerator. A dilution refrigerator is the only cryogenic system able to produce the required low temperatures continuously.
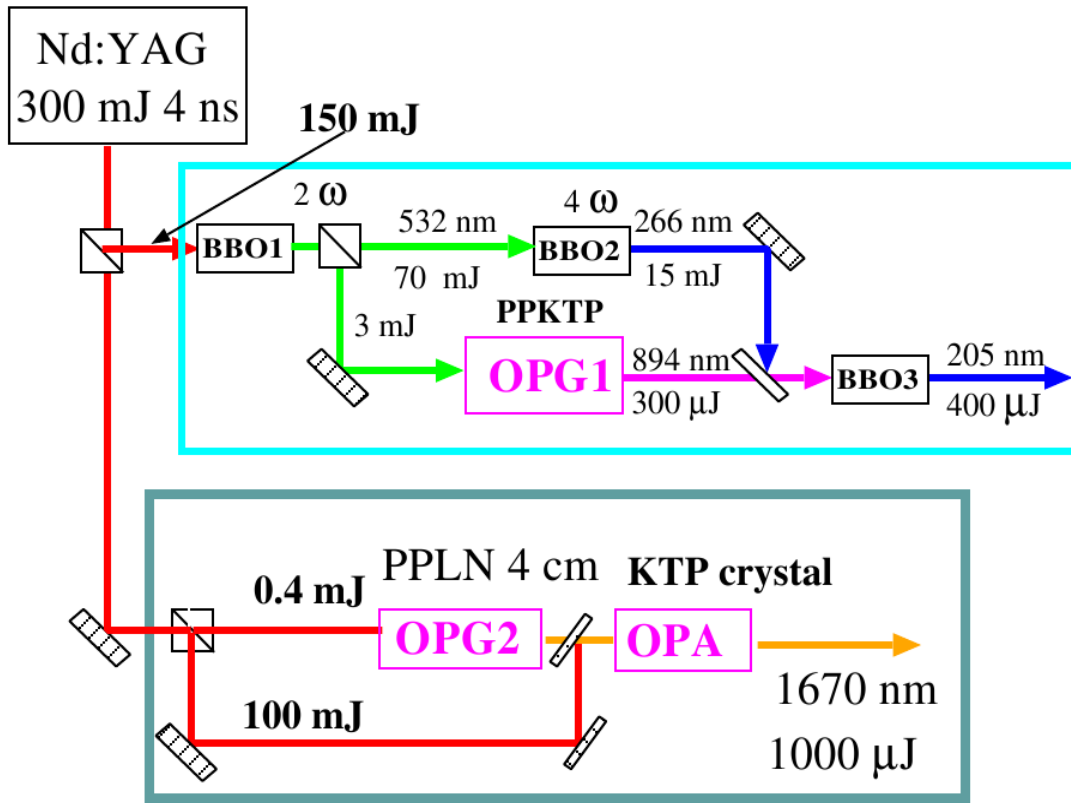
Figure 12. Sketch of the setup for the laser excitation of Rydberg positronium. The $n = 1 \rightarrow n = 3$ exciting laser at 205 nm is under development in Florence (turquoise box). The $n = 3 \rightarrow n = 20...30$ exciting laser at about 1670 nm has been realized in Milan (gray box).

In 2009, CERNs cryolab investigated the crucial thermal resistance between the ultra cold trap electrodes and the mixing chamber, which is the coldest part of the dilution refrigerator. These thermal resistances should be as low as possible. The electrodes will however be charged with different voltages (up to several kV) and should thus be individually electrically insulated. This electrical insulation implies however a poor thermal conduction. Further to consider are the thermal boundary resistances (Kapitza resistance), which increase significantly for ultra low temperatures.

There exist two mechanisms for transferring heat: phonons and electrons. In metals both mechanisms are present, with the heat transfer due to electrons being dominant. In dielectrics the heat is transferred only by phonons, which has the advantage of a very good electrical insulation. Keeping this in mind, we have investigated two options, which depend on different heat transfer mechanisms, to achieve this thermal conduction while maintaining electrical insulation: a first solution which puts individual electrodes into direct contact with the He^3/He^4 mixture within the mixing chamber ("rod solution"), and a second solution which involves coupling the electrodes to the copper surface of the mixing chamber through a thin sandwich of Indium-sapphire-Indium ("sandwich solution"), shown in Fig.13.

The metallic Rod connects a single electrode directly with the heat exchanger, located within the mixing chamber. The Rod passes through a ceramic, electrically insulating the electrode from the mixing chamber. The challenge of this design is the leak-tight brazed connection

between the Rod and the ceramic. A standardised brazing technique could not be applied, due to the use of magnetic materials in the standard brazing agent. These materials could influence the homogeneity of the high precision magnetic field, in which the mixing chamber is installed.

In contrast, the Sandwich design appears less problematic. The electrical insulation of the Sandwich is achieved by a sapphire plate, which is pressed between the electrode and the mixing chamber. To increase the thermal contact conductance, the sapphire plate is sandwiched in between two thin layers of Indium, which in turn make the contact between the electrode and the mixing chamber.

The thermal performances of the two designs have been measured, already with respect to the AEGIS environment. The preparation of the test setup included a number of activities, e.g. the calibration of thermometers, which are appropriate in a high magnetic field and sensitive down to ultra low temperatures; the design and manufacturing of the heat exchangers, already with a customised geometry and a special copper sinter matching the requirements of the temperature range; the design and the construction of a superconducting magnet, which is necessary to guarantee the normal state of indium, e.g. used in the Sandwich; and optimisation and preparation of the existing dilution refrigerator at CERNs cryolab, including an RF improved design.

Static and dynamic thermal measurements have been performed. During these measurements the heat load to the electrode was simulated with a heater and the temperatures of electrode and mixing chamber have been measured. The results show a significant difference of the thermal performances between Rod and Sandwich solutions. In Fig. 13 the impact of the different heat transfer mechanisms can clearly be seen. The Rod can transfer approx. 20 times more heat for the same occupied surface on the mixing chamber over a 50 mK temperature difference compared to the Sandwich. The occupied surface isnt the heat transferring cross section for the rod, but for the sandwich. These surfaces are calculated for the rod and the sandwich with the outer diameter of the electrical insulating ceramic and the diameter of the sapphire plate, respectively. The Sapphire solution is adequate for the requirements of AEGIS if a sufficiently large and good contact can be achieved for each segment of each electrode in the dilution refrigerator area, and a design is being worked on. Further investigations are also envisaged for the Rod solution. In particular, an open question concerns the electrical behavior of the ^{3}He-^{4}He mixture within the mixing chamber when the potential difference between two immersed rods is increased to ~1kV at the moment of Antihydrogen Stark acceleration. A further complication is the possible ionization of the He mixture under the influence of Ps annihilation radiation shortly prior to Stark acceleration. In the worst case, this could cause a breakdown of the dielectric properties of He.

2.7. Moiré deflectometer
We have now an optical interferometer of 2m length and corresponding readout for stabilization. We are currently implementing this set-up in a vacuum system to get rid of unwanted air motion. A working Moiré apparatus for atoms is expected to be ready by late summer.

3. Summary and outlook
Construction has started on the AEGIS experiment, whose design is based upon the broad experience gained with the ATHENA and ATRAP experiments at the AD. A series of ongoing tests and developments, as well as extensive simulations of critical processes (charge exchange production of $\bar{H}$, Stark acceleration and propagation through the Moiré deflectometer, resolution of the position-sensitive detector located at the end of the deflectometer) have validated most of the assumptions made in the proposal to the SPSC, but a small number of open questions
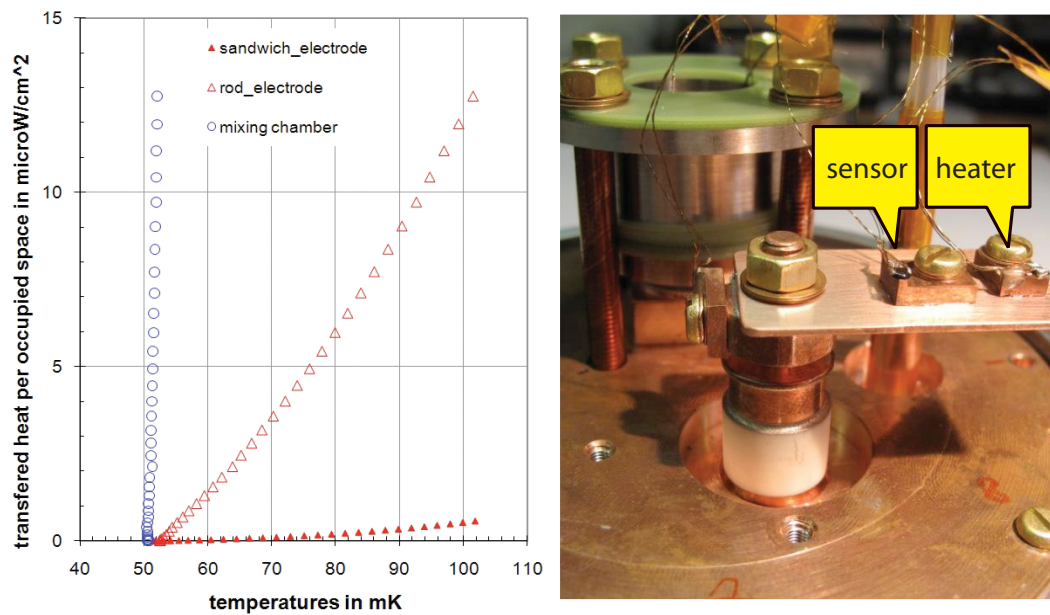
Figure 13. Left plot: Heat transfer for Sandwich (full triangles) and Rod (empty triangle) solutions. Shown is the heat transfer for the two solutions as a function of the temperature difference between the electrode and the mixing chamber. Right plot: Test set-up on the mixing chamber with the Rod solution (foreground) and sandwich solution (rear)

remain. Work is being carried out wherever possible to address these questions (Positronium emission and characterization at the final target temperature; laser excitation of positronium; stability, shielding and performance of the Moiré deflectometer) and results are expected in the course of the year, but a certain number of questions will only be addressable in the complete apparatus. Among these are the final temperature of the antiprotons in the dilution refrigerator region, the pulsed formation of antihydrogen atoms, their characterization and the formation of an antihydrogen beam.

[1] http://cdsweb.cern.ch/search?of=hd&p=reportnumber:CERN-SPSC-2007-017
[2] L.V. Jorgensen et al., ATHENA Collaboration, Phys. Rev. Lett. 95 (2005) 025002.
[3] G. Gabrielse et al., ATRAP Collaboration, Phys. Lett. B 548 (2002) 140.
[4] M. Charlton, Phys. Lett. A 143 (1990) 143.
[5] B.I. Deutch et al., Hyperfine Interact. 76 (1993) 153.
[6] G. Gabrielse et al., ATRAP Collaboration, Phys. Rev. Lett. 93 (2004) 073401
[7] N. Madsen et al., ATHENA Collaboration, Phys. Rev. Lett. 94 (2005) 033403
[8] E.A. Hessels, D.M. Homan, M.J. Cavagnero, Phys. Rev. A 57 (1998) 1668
[9] C.H. Storry et al., ATRAP Collaboration, Phys. Rev. Lett. 93 (2004) 263401
[10] E. Vliegen, F. Merkt, J. Phys. B 39 (2006) L241.
[11] E. Vliegen et al., Phys. Rev. A 76 (2007) 023405.
[12] L. Zehnder, Z. Instrumentenkunde 11 (1891) 275.
[13] L. Mach, Z. Instrumentenkunde 12 (1892) 89.
[14] M.K. Oberthaler et al., Phys. Rev. A 54 (1996) 3165.
[15] J. Fajans, E. Gilson and L. Friedland Phys. Rev. Lett. 82:4444, 1999.
[16] D.W. Gidley, H.-G. Peng, R.S. Vallery, Annu. Rev. Mater. Res. 36 (2006) 49

[17] C. Canali, publication in preparation.

[18] S. Mariazzi, A. Salemi, R. Brusa, Phys. Rev. B 78 (2008) 085428.

[19] F. Castelli, I. Boscolo, S. Cialdi and M. G. Giammarchi, Phys. Rev. A **78** (2008) 052512.

[20] R. Ferragut et al., talk at the Advanced Science Research Symposium 2009, Tokai (Japan), November 2009

[21] N. Djourelov , C A Palacio, J De Baerdemaeker, C Bas, N Charvin, K De- lendik, G Drobychev, D Sillou, O Voitik and S Gninenko. J. Phys.: Condens. Matter 20 (2008)